Available online at www.sciencedirect.com
SCIENCE DIRECT®
Journal of Solid State Chemistry 178 (2005) 114–119
JOURNAL OF SOLID STATE CHEMISTRY
www.elsevier.com/locate/jssc

Structural and magnetic properties of $Ba_3La_3Mn_2W_3O_{18}$

Zhaofei Li[a], Junliang Sun[a], Yingxia Wang[a], Liping You[b], Jian-Hua Lin[a,*]

[a]*State Key Laboratory of Rare Earth Materials Chemistry and Applications, Department of Material Chemistry, College of Chemistry and Molecular Engineering, Peking University, Beijing 100871, PR China*
[b]*Electron Microscopy Laboratory, College of Physics, Peking University, Beijing 100871, PR China*

Received 14 September 2004; received in revised form 31 October 2004; accepted 7 November 2004
Available online 8 December 2004

Abstract

A quaternary phase, $Ba_3La_3Mn_2W_3O_{18}$, was synthesized in reduced atmosphere (5% H_2/Ar) at 1200 °C and characterized by using powder X-ray diffraction, electron diffraction and high resolution TEM. $Ba_3La_3Mn_2W_3O_{18}$ crystallizes in rhombohedral space group $R\bar{3}m$ with the cell parameters, $a = 5.7371(1)$ Å and $c = 41.8336(5)$ Å, and can be attributed to the $n = 6$ member in the B-site deficient perovskite family, $A_nB_{n-1}O_{3n}$. The structure can be described as close-packed [La/BaO_3] arrays in the sequence of $(hcccch)_3$, wherein the B-site cations, W and Mn, occupy five octahedral layers in every six octahedral layers, which leave a vacant octahedral layers separating the 5-layer perovskite blocks. The B-cation layers in the perovskite block alternate along the *c*-axis in a sequence of W^{6+}–Mn^{2+}–W^{5+}–Mn^{2+}–W^{6+}. The bond valence calculation and optical reflection spectrum confirm the presence of W^{5+}. This compound behaves paramagnetically in wide temperature range and weak antiferromagnetic interaction only occurs at low temperatures.

Keywords: Deficient perovskite; Layered structure; XRD; Electron microscopy

1. Introduction

Intergrowth of perovskite block and other motif may lead to various structure types. A well-known example is the Ruddlesden-Popper phase $(ABO_3)_nAO$ [1] which consists of perovskite and rock salt blocks. A hexagonal perovskite intergrowth family identified recently, $A_nB_{n-1}O_{3n}(A_2'O)$ [2–9], contains hexagonal perovskite blocks and a graphite-like sheet [A_2'O]. Another related hexagonal perovskite family is the $A_nB_{n-1}O_{3n}$, which could be considered as deficient derivatives in removing the [A_2'O] sheet from the $A_nB_{n-1}O_{3n}(A_2'O)$ family. Many compounds with this structure type have been known, such as binary $La_nTi_{n-1}O_{3n}$ [10] and $Ba_5Nb_4O_{15}$ [12], ternary $Ba_5SrTa_4ZrO_{18}$, $Ba_5Sr_2Ta_4Zr_2O_{21}$, $Ba_5Sr_3Ta_4Zr_3O_{24}$ [11], $La_4BaTi_4O_{15}$, $La_4Ba_2Ti_5O_{18}$ [13], $Ba_6TiNb_4O_{18}$ [12] and even quaternary systems $Ba_3La(InW_2O_{12})$, $Ba_2La_2B^{II}W_2^{VI}O_{12}$ (B = Mg, Zn, Co, Cu), $Ba_4(B^{III}ReWO_{12})$ (B = Sc, In, Lu), $Ba_4Mg(Re_2O_{12})$ and $Ba_4Cd(Re_2O_{12})$ [14,15]. The structures of these compounds can be described as stacking the hexagonal perovskite blocks of the $n-1$ octahedra thick along the *c*-axis that leaves a *B*-vacant layer [10–12]. Most of such compounds crystallize in either rhombohedral or primitive trigonal symmetry and, according to the rules proposed by Abakumov et al. [11], the structure has the primitive trigonal symmetry if $n-2 = 3m$ (m is an integer), otherwise, it has rhombohedral symmetry. Recently, we obtained a manganese-containing compound, $Ba_2La_2MnW_2O_{12}$, which is an $n = 4$ member of the A_nBO_{3n} family [16]. This compound was synthesized by high-temperature solid-state reaction in reduced atmosphere (4% H_2/Ar). By systematic study, we identified another member in this system, $Ba_3La_3Mn_2W_3O_{18}$. In this paper, we report the structural and magnetic properties of this phase.

*Corresponding author. Fax: +86 10 6275 1708.
E-mail address: jhlin@pku.edu.cn (J.-H. Lin).

0022-4596/$ - see front matter © 2004 Elsevier Inc. All rights reserved.
doi:10.1016/j.jssc.2004.11.007

2. Experimental

$Ba_3La_3Mn_2W_3O_{18}$ was synthesized by the following procedure. The starting materials, La_2O_3 and WO_3, were pretreated at 700 °C and $BaCO_3$ at 200 °C for 6 h to remove the absorbed H_2O and CO_2. Mixture with a ratio of La_2O_3: $BaCO_3$: $MnCO_3$: $WO_3 = 1.5:3:2:3$ was ground thoroughly in ethanol and then preheated in air at 950 °C for 6 h. The powder was pressed into pellets and sintered at 1200 °C for 3 h in 5%H_2/Ar flow. The pressing and heating procedures were repeated several times until the product was essentially a single phase.

Powder X-ray diffraction data was collected at room temperature on a Bruker D8 Advance diffractometer with a curved germanium primary monochromator (Cu$K\alpha_1$, $l = 1.5406$ Å) using a transmission sample holder and a PSD detector (4° 2θ window). The data was collected in the range of 5–130° with a step scanning mode, and the step scan size and time are: 0.0144 (2θ) and 30 s. Tube voltage and current were kept at 50 kV and 40 mA, respectively. Electron diffraction and high-resolution TEM were carried out on a Hitachi H-9000 electron microscope. Optical reflection spectrum was measured with a Shimado UV-3100 Spectrometer in range from 200 to 3200 nm. Magnetic susceptibility was measured on a Maglab System 2000 magnetometer (Oxford Instruments). The experimental susceptibilities were corrected for diamagnetism of the constituent atoms (Pascal's tables).

3. Results and discussion

Fig. 1 shows the X-ray powder diffraction pattern of $Ba_3La_3Mn_2W_3O_{18}$. The diffraction pattern of $Ba_2La_2MnW_2O_{12}$ is also included for comparison. It has been known that $Ba_2La_2MnW_2O_{12}$ crystallizes in rhombohedral space group $R\bar{3}m$ with $a = 5.7276(3)$ Å and $c = 27.393(2)$ Å [16]. The X-ray diffraction pattern of $Ba_3La_3Mn_2W_3O_{18}$ can also be indexed with a hexagonal cell, $a = 5.7371(1)$ Å and $c = 41.834(5)$ Å. The systematic absence of the reflections $-h+k+l \neq 3n$ revealed rhombohedral symmetry for $Ba_3La_3Mn_2W_3O_{18}$ and, the possible space groups include $R\bar{3}m$, $R3m$, $R\bar{3}$, $R3$ or $R32$. The rhombohedral symmetry of the $Ba_3La_3Mn_2W_3O_{18}$ structure was further supported by electron diffraction (ED) studies. In Fig. 2, we show the ED patterns of $Ba_3La_3Mn_2W_3O_{18}$ along the [010], [1$\bar{1}$0] and [001] directions. All of the ED patterns can be indexed with the rhombohedral cell as that from X-ray diffraction study.

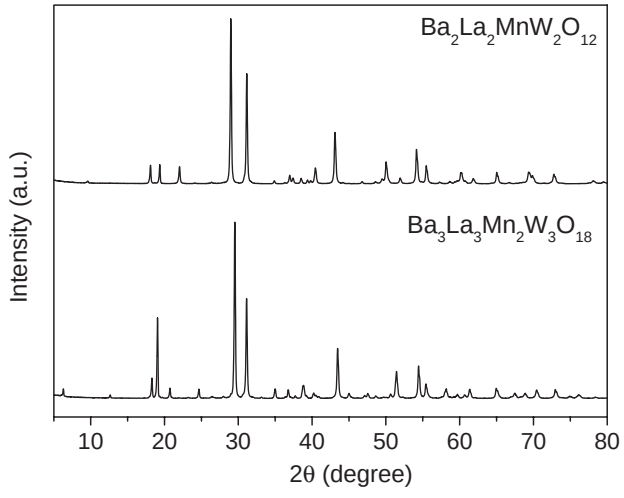

Fig. 1. X-ray diffraction patterns of $Ba_2La_2MnW_2O_{12}$ and $Ba_3La_3Mn_2W_3O_{18}$.

The structure model was initially studied by the direct method with EXPO, in which the individual reflection intensities were extracted by EXTRA [17] and parts of atomic positions were revealed with Sirpow92 [18]. The cation positions were located directly from the E-map that suggested chemical formula $A_6B_5O_{18}$ for this compound. By careful comparison of the atomic sites and diffraction pattern, we realized $Ba_3La_3Mn_2W_3O_{18}$ is in fact isostructural with a known compound $Ba_5SrTa_4ZrO_{18}$ [11]. Therefore, the structure of $Ba_5SrTa_4ZrO_{18}$ was then used as a starting set for the structure refinement. The structure refinement was carried out by Rietveld method with GSAS [19]. A six-term Cosine Fourier series was used for the background and the pseudo-Voigt function was used to model the peak profile. The refinement indicated that Mn and W atoms are partially ordered at the B sites in this $A_6B_5O_{18}$ structure, which, unlike to $Ba_5SrTa_4ZrO_{18}$ where the Ta and Zr atoms are randomly distributed. In Fig. 3 we show the profile fitting of the powder diffraction pattern. The atomic coordinates and selected bond lengths are summarized in Tables 1 and 2, respectively.

Fig. 4 shows the structure of $Ba_3La_3Mn_2W_3O_{18}$ projected along [110] direction. The structure can be described as successive stacking of a five-octahedra-thick perovskite block along the c-axis, which leaves a vacant octahedral layer between the perovskite blocks. The three crystallographically independent octahedral sites are occupied by Mn, W1 and W2 in a fashion that the [MnO_6] and [WO_6] octahedral layers alternate along the c-axis. Alternatively, the structure can also be described by close-packed [(La/Ba)O_3] layers, in which the manganese and tungsten atoms locate in the octahedral sites. In Jagodzinski' notation, the sequence of the [(La/Ba)O_3] layers is $(hcccch)_3$ [20]. One could see that the octahedral sites between the two adjacent h–type layers are vacant due to the strong electric repulsion of the W ions. As a consequence, the W–O distances toward the vacant layer are shorter (W2–O1: 1.807 Å) than those toward the Mn layer (W2–O2: 2.075 Å).

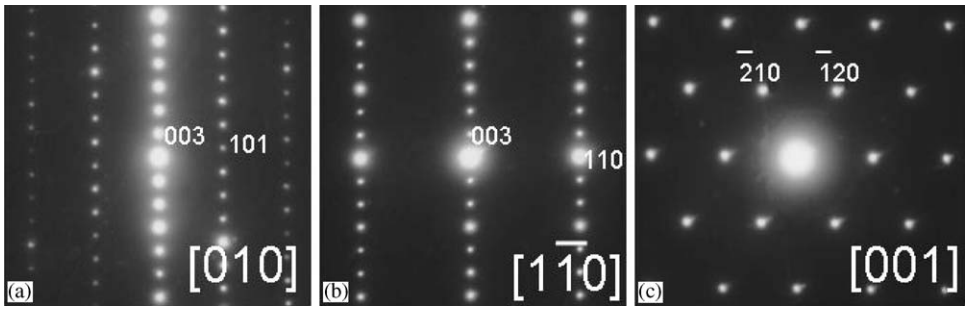

Fig. 2. Electron diffraction patterns of $Ba_3La_3Mn_2W_3O_{18}$ along (a) [010], (b) [1$\bar{1}$0] and (c) [001] directions.

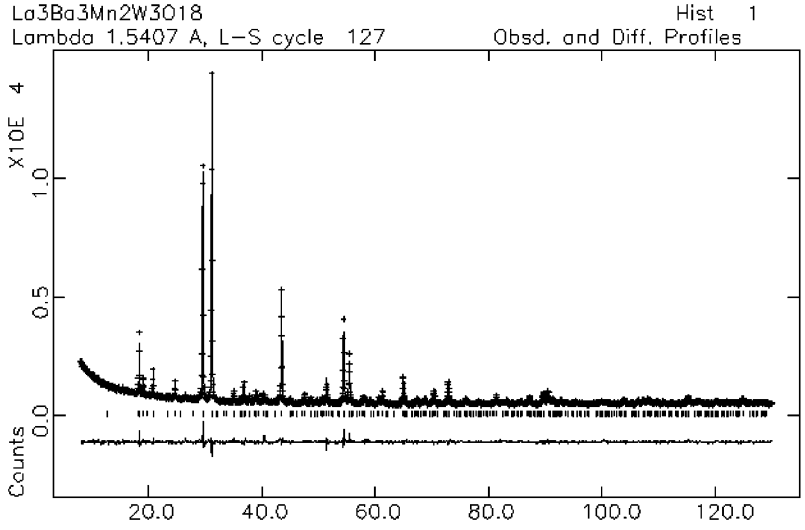

Fig. 3. Observed (+) and calculated (solid line) X-ray powder diffraction pattern of $Ba_3La_3Mn_2W_3O_{18}$. The difference plot is located at the bottom. The small bars are the reflection positions.

Table 1
Atomic parameters of $Ba_3La_3Mn_2W_3O_{18}$ at room temperature

Space group: $R\bar{3}m$, Lattice constants: $a = 5.7371(1)$ Å, $c = 41.8336(5)$ Å
The refined figures: $R_p = 0.0385$; $R_{wp} = 0.0509$; $x^2 = 1.880$

Atom	Wyckoff site	x	y	z	Occupation	B_{iso}/Å^2
$M1^*$	6c	0	0	0.0849(2)	1.0	1.32
$M2^*$	6c	0	0	0.1877(2)	1.0	1.32
$M3^*$	6c	0	0	0.3625(2)	1.0	1.32
W1	3a	0	0	0	1.0	1.27
W2/Mn	6c	0	0	0.4470(1)	0.95/0.05	0.92
Mn1/W	6c	0	0	0.2756(4)	0.95/0.05	1.06
O1	18h	0.1773(13)	−0.1773(13)	0.1358(6)	1.0	2.44
O2	18h	0.1762(20)	−0.1762(20)	0.2524(5)	1.0	2.44
O3	18h	0.1731(19)	−0.1731(19)	0.6898(7)	1.0	2.44

*$M = 0.5$Ba + 0.5La.

Fig. 5 shows the high-resolution TEM image of $Ba_3La_3Mn_2W_3O_{18}$ in the [110] zone. It can be seen that the perovskite blocks alternate with vacant layers along the c-axis. The repeating unit along the c-direction covers three perovskite blocks that give rise to the c-parameter of about 41.7 Å. In fact, one could estimate the lattice constants of the $A_nB_{n-1}O_{3n}$ family by using the following relationship, $a \approx \sqrt{2}a_c$ and $c \approx \sqrt{3}na_c$,

Table 2
Selected bond lengths in $Ba_3La_3Mn_2W_3O_{18}$

Bond	Mult.	Length (Å)	Bond	Mult.	Length (Å)
M1–O1	3	2.766(23)	M3–O3	6	2.8804(24)
M1–O2	6	2.8748(16)	M3–O3	3	2.782(27)
M1–O3	3	3.035(29)	Mn–O2	3	2.003(20)
M2–O1	3	2.795(22)	Mn–O3	3	2.247(23)
M2–O1	6	2.8996(35)	W1–O3	6	1.863(18)
M2–O2	3	3.224(24)	W2–O1	3	1.807(21)
M3–O2	3	2.670(24)	W2–O2	3	2.075(19)
The mean bond lengths (Å):					
M1–O	2.888	M2–O	2.955	M3–O	2.803
Mn–O	2.125	W1–O	1.863	W2–O	1.941

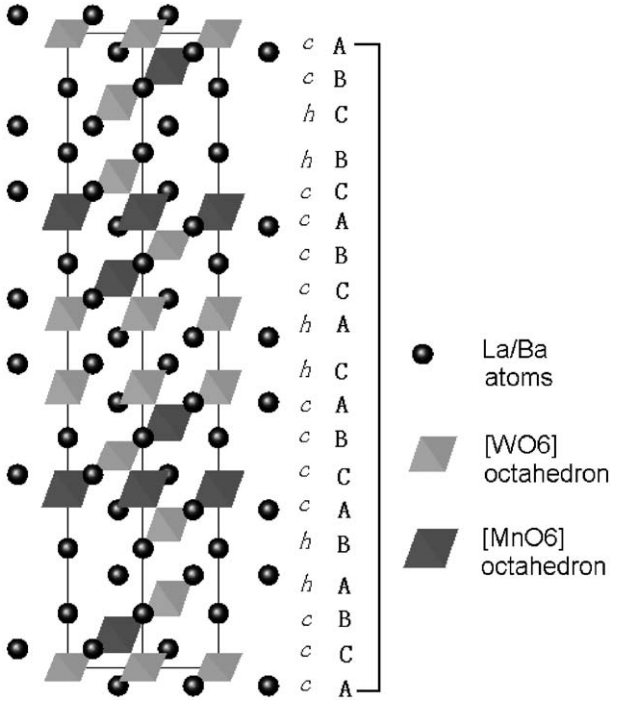

Fig. 4. Crystal structure of $Ba_3La_3Mn_2W_3O_{18}$ viewed along the [110] direction. Dark octahedra are the [MnO_6], and light ones are [WO_6]. And the dark spheres represent the Ba and La atoms.

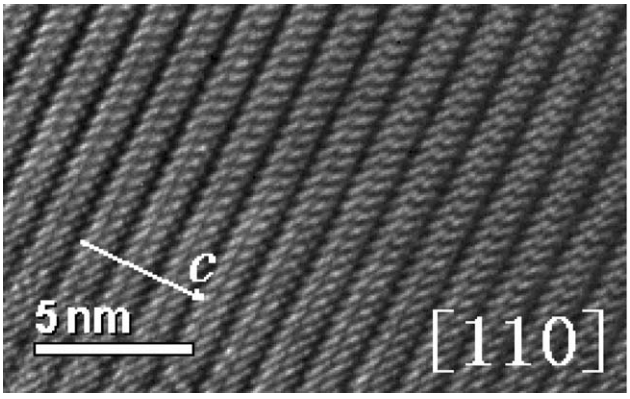

Fig. 5. HRTEM image of $Ba_3La_3Mn_2W_3O_{18}$ in the [110] zone.

where the a_c is the lattice constant of cubic perovskite. The lattice constants estimated from these expressions are $a \approx 5.6$ Å and $c \approx 41.6$ Å for $Ba_3La_3Mn_2W_3O_{18}$ ($n = 6$) and $a \approx 5.6$ Å and $c \approx 27.7$ Å for $Ba_2La_2MnW_2O_{12}$ ($n = 4$), which agree with the observed lattice parameters reasonably well. This relationship can also be used to interpret the high-resolution TEM images of these structures (Fig. 5) [16].

To estimate the formal oxidation state of the cations, we calculated the bond valence in the structure of $Ba_3La_3Mn_2W_3O_{18}$. The result shows that the manganese ions are most likely in +2 (+2.27). Meanwhile, the two tungsten atoms (W1 and W2) are, respectively, in +5 (+4.89) and +6 (+6.16). Furthermore, the charges are ordered in the structure, i.e., the W^{6+} ions are located mostly on the surface of the perovskite block, whereas the W^{5+} ions are mainly at the central octahedral layer. The presence of W^{5+} ions in $Ba_3La_3Mn_2W_3O_{18}$ is further supported by absorption spectrum shown in Fig. 6. Both $Ba_2La_2MnW_2O_{12}$ and $Ba_3La_3Mn_2W_3O_{18}$ show strong absorption for $\lambda < 580$ nm. For $Ba_3La_3Mn_2W_3O_{18}$, an absorption shoulder appears at about 600–700 nm, which may attribute to transition related to the $5d^1$ configuration of the W^{5+} ions. The La^{3+} and Ba^{2+} atoms are distributed with three different sites, all of which are twelve-coordinated. The structure refinement cannot differentiate lanthanum and barium. However, the averaged M2–O bond distance (2.9545 Å) is significantly larger than M1–O (2.8877 Å) and M3–O (2.8032 Å), indicating that Ba prefer to reside in the M2 site and the La and the rest of the Ba atoms may randomly be distributed within the M1 and M3 sites. The bond valence calculation indicates a similar trend (the BVS calculation results are 2.464, 2.16 and 3.08 for M1, M2 and M3, respectively).

$Ba_3La_3Mn_2W_3O_{18}$ is an $n = 6$ member in the $A_nB_{n-1}O_{3n}$ family [8–10]. In comparison with the hexagonal intergrowth family $A_nB_{n-1}O_{3n}(A_2'O)$, the graphite-like [Ca_2O] layers are missing in this *B*-deficient family $A_nB_{n-1}O_{3n}$. Since the vacant octahedral layers interrupt magnetic interaction between the

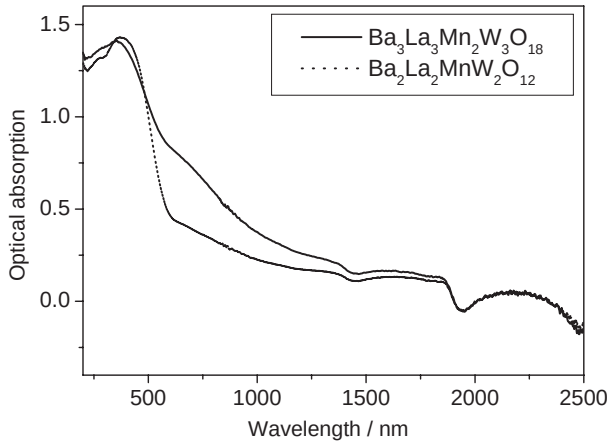

Fig. 6. Optical absorption spectra of $Ba_2La_2MnW_2O_{12}$ and $Ba_3La_3Mn_2W_3O_{18}$.

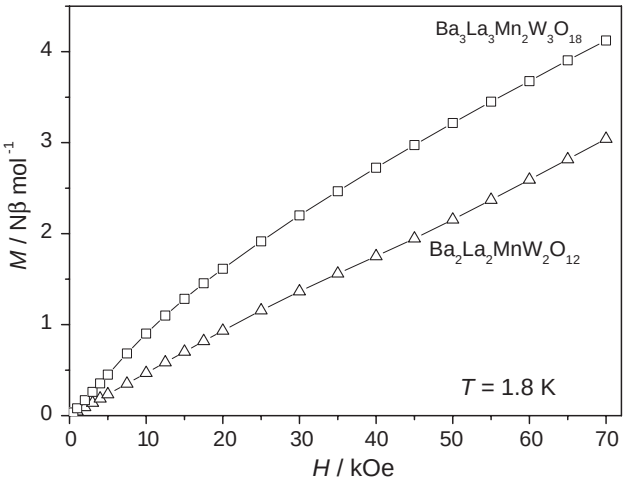

Fig. 8. M versus H plot at 1.8 K for $Ba_2La_2MnW_2O_{12}$ and $Ba_3La_3Mn_2W_3O_{18}$.

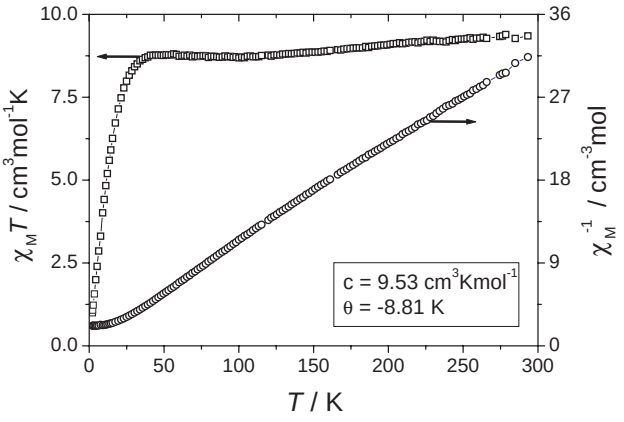

Fig. 7. The $\chi_M T$ and $1/\chi_M$ versus T plots for $Ba_3La_3Mn_2W_3O_{18}$.

transition metals, these compounds may behave local magnetic interactions. In Fig. 7 we show the $\chi_M T$ and $1/\chi_M$ plots for $Ba_3La_3Mn_2W_3O_{18}$ under 20 kOe of applied magnetic field (in the CGS system). The molar magnetic susceptibility χ_M obeys the Curie–Weiss law with $C = 9.53\,\mathrm{cm^3\,mol^{-1}\,K}$ and $\theta = -8.81\,\mathrm{K}$; and a slight deviation is observed at low temperature. The negative Weiss constant indicates weak antiferromagnetic interaction inside this compound. The $\chi_M T$ value at room temperature is $9.1\,\mathrm{cm^3\,mol^{-1}K}$ (per f. u.), which is very close to the value of $9.125\,\mathrm{cm^3\,mol^{-1}\,K}$ calculated for uncoupled two $S = \frac{5}{2}$ spins and one $S = \frac{1}{2}$ spins, which further confirm the valence state of those elements in this compound. Fig. 8 shows the M–H plot for $Ba_3La_3Mn_2W_3O_{18}$ at 1.8 K. The M–H curve of $Ba_2La_2MnW_2O_{12}$ is also included for comparison. It can be seen that both compounds behave predominantly as paramagnetic systems. Weak antiferromagnetic interaction may exist as indicated by bending of the M–H curves. From the structure of $Ba_3La_3Mn_2W_3O_{18}$, we knew the $[W^{5+}O_6]$ layer is sandwiched by two $[Mn^{2+}O_6]$ layers, thus the predominant paramagnetic behavior of this compound may mean the magnetic interaction between those cations is very week in this compound.

In conclusion, a new quaternary compounds, $Ba_3La_3Mn_2W_3O_{18}$, was synthesized in reduced atmosphere. This compound is an $n = 6$ member in the B-site deficiency family of $A_nB_{n-1}O_{3n}$, consisting of successive stacking of a five-octahedra-thick perovskite blocks. Within the perovskite block, the W- and Mn-octahedra layers are ordered and alternated along the c-axis. The magnetic susceptibility and absorption spectra all indicate the presence of W^{5+}.

Acknowledgments

We are thankful for the financial support from NSFC (20221101 and 20371005).

References

[1] G.B. Hyde, S. Anderson, Inorganic Crystal Structures, Wiley, New York, 1989.
[2] Y.X. Wang, J.H. Lin, Y. Du, R.W. Qin, B. Han, C.K. Loong, Angew. Chem. 112 (2000) 2842;
Y.X. Wang, J.H. Lin, Y. Du, R.W. Qin, B. Han, C.K. Loong, Angew. Chem. Int. Ed. 39 (2000) 2730.
[3] L.J. Bie, J.H. Lin, Y.X. Wang, C.K. Loong, Inorg. Chem. Comm. 5 (2002) 966.
[4] L.J. Bie, Y.X. Wang, J.H. Lin, C.K. Loong, J.W. Richardson Jr, L.P. You, C. Dong, Chem. Mater. 15 (2003) 516.
[5] S.G. Ebbinghaus, J. Solid State Chem. 177 (2004) 817–823.
[6] K.E. Stitzer, J. Darriet, H.-C. zur Loye, Curr. Opin. Solid State Mater. Sci. 5 (2001) 535.
[7] F. Grasset, M. Zakhour, J. Darriet, J. Alloys Compd. 25 (1999) 287.

[8] C. Dussarrat, J. Fompeyrine, J. Darriet, Eur. J. Solid State Inorg. Chem. 31 (1994) 289.
[9] E. Gaudin, G. Goglio, A. Besnard, J. Darriet, J. Solid State Chem. 175 (2003) 124.
[10] G. Van Tendeloo, S. Amelinckx, B. Darriet, R. Bontchev, J. Darriet, F. Weill, J. Solid State Chem. 108 (1994) 314.
[11] A.M. Abakumov, R.V. Shpanchenko, E.V. Antipov, O.I. Lebedev, G. Van Tendeloo, S. Amelinckx, J. Solid State Chem. 141 (1998) 492.
[12] G. Trolliard, N. Teneze, Ph. Boullay, M. Manier, D. Mercurio, J. Solid State Chem. 173 (2003) 91.
[13] C. Vineis, P.K. Davies, T. Negas, S. Bell, Mat. Res. Bull. 31 (1996) 431.
[14] Von.S. Kemmler-Sack, Z. Anorg. Allg. Chem. 461 (1980) 142.
[15] V.H.J. Rother, A. Fadini, S. Kemmler-Sack, Z. Anorg. Allg. Chem. 463 (1980) 137.
[16] Z.F. Li, J.L. Sun, L.P. You, Y.X. Wang, J.H. Lin, J. Alloys Compd. 379 (2004) 117.
[17] A. Altomare, M.C. Burla, G. Cascarano, C. Giacovazzo, A. Guagliardi, A.G.G. Moliterni, G. Polidori, J. Appl. Cryst. 28 (1995) 842.
[18] A. Altomare, G. Cascarana, C. Giacovazzo, A. Guagliardi, SIRPOW user's manual; Inst. Di Ric. Per lo Sviluppo di Metodologie Cristallografiche, CNR.
[19] A.C. Larson, R.B. von Dreele, report LAUR 86-748, Los Alamos National Laboratory, 1985.
[20] H. Jagodzinski, Acta Crystallogr. 2 (1949) 201.